AFRL-RV-PS-
TR-2013-0135

MOMENT-PRESERVING COMPUTATIONAL APPROACH FOR HIGH ENERGY CHARGED PARTICLE TRANSPORT

Second Interim Performance Report

Anil K. Prinja
David A. Dixon

University of New Mexico
Chemical and Nuclear Engineering Department
MSC01 1120, 209 Farris Engineering Center
Albuquerque, NM 87131

6 November 2013

Interim Report

AIR FORCE RESEARCH LABORATORY
Space Vehicles Directorate
3550 Aberdeen Ave SE
AIR FORCE MATERIEL COMMAND
KIRTLAND AIR FORCE BASE, NM 87117-5776

DTIC COPY

NOTICE AND SIGNATURE PAGE

Using Government drawings, specifications, or other data included in this document for any purpose other than Government procurement does not in any way obligate the U.S. Government. The fact that the Government formulated or supplied the drawings, specifications, or other data does not license the holder or any other person or corporation; or convey any rights or permission to manufacture, use, or sell any patented invention that may relate to them.

This report was cleared for public release by the 377 ABW Public Affairs Office and is available to the general public, including foreign nationals. Copies may be obtained from the Defense Technical Information Center (DTIC) (http://www.dtic.mil).

AFRL-RV-PS-TR-2013-0135 HAS BEEN REVIEWED AND IS APPROVED FOR PUBLICATION IN ACCORDANCE WITH ASSIGNED DISTRIBUTION STATEMENT.

//SIGNED//	//SIGNED//
Adrian Wheelock Program Manager/ AFRL/RVBXR	Edward J. Masterson, Colonel, USAF Chief, Battlespace Environment Division

This report is published in the interest of scientific and technical information exchange, and its publication does not constitute the Government's approval or disapproval of its ideas or findings.

REPORT DOCUMENTATION PAGE

Form Approved
OMB No. 0704-0188

1. REPORT DATE *(DD-MM-YYYY)*	**2. REPORT TYPE**	**3. DATES COVERED** *(From - To)*
06-11-2013	Interim Report	01 May 2012 to 01 May 2013

4. TITLE AND SUBTITLE
MOMENT-PRESERVING COMPUTATIONAL APPROACH FOR HIGH ENERGY CHARGED PARTICLE TRANSPORT
Second Interim Performance Report

5a. CONTRACT NUMBER
FA9453-11-1-0276

5b. GRANT NUMBER

5c. PROGRAM ELEMENT NUMBER
62601F

6. AUTHOR(S)
Anil K. Prinja and David A. Dixon

5d. PROJECT NUMBER
1010

5e. TASK NUMBER
PPM 00011354

5f. WORK UNIT NUMBER
EF004076

7. PERFORMING ORGANIZATION NAME(S) AND ADDRESS(ES)

University of New Mexico
Chemical and Nuclear Engineering Department
MSC01 1120, 209 Farris Engineering Center
Albuquerque, NM 87131

8. PERFORMING ORGANIZATION REPORT NUMBER

9. SPONSORING / MONITORING AGENCY NAME(S) AND ADDRESS(ES)

Air Force Research Laboratory
Space Vehicles Directorate
3550 Aberdeen Avenue SE
Kirtland AFB, NM 87117-5776

10. SPONSOR/MONITOR'S ACRONYM(S)
AFRL/RVBXR

11. SPONSOR/MONITOR'S REPORT NUMBER(S)
AFRL-RV-PS-TR-2013-0135

12. DISTRIBUTION / AVAILABILITY STATEMENT

Approved for public release; distribution is unlimited. (377ABW-2013-0490 dtd 11 Jun 2013)

13. SUPPLEMENTARY NOTES

14. ABSTRACT

An algorithm for generating Generalized Boltzmann Fokker-Plank (GBFP) discrete cross-section data and the implementation of the discrete model in Geant4 are described. Comparisons of angular distributions generated by the analog and discrete models are presented. Moreover, a case is made for implementation of the GBFP hybrid model to mitigate the discrete artifacts highlighted in the aforementioned comparison. Comparisons of dose profiles generated by the analog and discrete models are presented.

15. SUBJECT TERMS
Reduced Physics Models, Geant4, CEASE, MCNPX

16. SECURITY CLASSIFICATION OF:			**17. LIMITATION OF ABSTRACT**	**18. NUMBER OF PAGES**	**19a. NAME OF RESPONSIBLE PERSON**
a. REPORT	**b. ABSTRACT**	**c. THIS PAGE**			Adrian Wheelock
Unclassified	Unclassified	Unclassified	Unlimited	26	**19b. TELEPHONE NUMBER** *(include area code)*

This page is intentionally left blank.

Table of Contents

List of Figures

1. INTRODUCTION

The following sections present work completed under the UNM/AFRL research grant FA9453-11-1-0276 since May 2012. During this time period, the majority of the research completed was the development and implementation of analog physics models and advanced single-event physics models in Geant4 [1]. A Geant4 model of the CEASE detector was completed that will be used for future testing and simulations.

2. BACKGROUND

In Monte Carlo simulation of the transport of charged particles, the analog and advanced single-event physics models require total and differential interaction cross-sections, which are used to sample the particle distance to collision, scattering angle, and energy-loss. One example of the transport equation for electrons that can undergo angular deflection and energy-loss interactions is given by

$$\vec{\Omega}\cdot\nabla\psi(E,\vec{\Omega})+\Sigma_t\psi(E,\vec{\Omega})=\int_{4\pi}\Sigma_n(E,\mu_0)\psi(E',\vec{\Omega}')d\Omega'+\int_{Q_{min}}^{Q_{max}}\Sigma_{e^-}(E+Q,Q)\psi(E+Q,\vec{\Omega})dQ. \quad (1)$$

Solution to this equation using the Monte Carlo method will give an exact solution within statistics. In a given material, distance to collision is sampled from

$$P(s)ds=\Sigma_t\exp(-\Sigma_t s)ds. \quad (2)$$

Angular deflection and energy-loss are sampled from their respective cross-sections that are both characterized by the Rutherford cross-section in their most simple form. The Rutherford cross-section for angular deflection is

$$\Sigma_s(\vec{r},E,\mu_0)=\frac{C(E)}{[1-\mu_0+2\eta(E)]^2}\ . \quad (3)$$

The Rutherford cross-section for energy-loss is

$$\Sigma_{e^-}(E,Q)=\frac{K(E)}{\beta^2Q^2} \quad (4)$$

where C(E) and K(E) are material constants. There are several cross-sections that are more accurate than the Rutherford cross-sections and typically used in practice (like the Mott cross-section and the Moller cross-section). Regardless, the Rutherford cross-sections in eq. 3 and eq. 4 illustrate the peakedness of the cross-sections near forward angles and small energy losses. In addition the total cross-sections are large. Cross-sections of this nature make Monte Carlo simulations extremely computationally inefficient and impractical, as detailed in the statement of work [6]. The advanced single-event physics models, referred to in the following sections as the Generalized Boltzmann Fokker-Plank method (GBFP), are based on powerful results from Lewis theory [2] and higher-order Fokker-Plank expansions [8] [9]. To summarize the connection of the theory to the GBFP method, nearby or approximate forms of the analog TE are formed using

approximate forms of the cross-section. The approximate cross-sections should preserve a finite number of angular and energy-loss moments of the analog cross-section. Increasing the number of moments preserved results in an increasingly more accurate approximation. This approximate transport equation is solved using existing single-event Monte Carlo simulation techniques. The moments are defined by

$$M_l = 2\pi \int_{-1}^{1} P_l(\mu)\Sigma_s(\vec{r},E,\mu)d\mu \tag{5}$$

and

$$\nu_k = \int_{Q_{min}}^{Q_{max}} Q^k \Sigma_{e^-}(\vec{r},E,Q)dQ \tag{6}$$

where $P_l(\mu)$ is the Legendre polynomial of degree l and Q^k is a power moment. The cross-sections used in the GBFP method are obtained by forming a system of equations to determine discrete points and weights or function parameters such that a finite number of moments are preserved. For example, to obtain a discrete GBFP cross-section the following system is formed

$$M_l = \tilde{M}_l = 2\pi \int_{-1}^{1} P_l(\mu)\tilde{\Sigma}_s(\vec{r},E,\mu)d\mu \tag{7}$$

where $\tilde{\Sigma}_s$ is a discrete cross-section given by

$$\tilde{\Sigma}_s(E,\mu) = \sum_{n=1}^{N} \frac{\alpha_n(E)}{2\pi}\delta[\mu_0 - \xi_n]. \tag{8}$$

Inserting this expression into eq. (7) gives

$$M_l = \sum_{n=1}^{N} P_l(\xi_n)\alpha_n(E). \tag{9}$$

The system in eq. (9) is a 2N by 2N system where the M_l's are assumed to be known and the discrete points and weights, ξ_n and α_n, are determined using Gaussian Quadrature methods. Details on the algorithm to obtain a discrete cross-section are given in the following section. The discrete cross-sections are then used in Monte Carlo simulation to obtain dose deposition and angular distribution results and compared to the exact analog solutions.

3. METHODS, PROCEDURES, AND ASSUMPTIONS

3.1. GBFP Discrete Cross-section Generation

Over the past reporting period, a method for obtaining a solution to eq. (9) was implemented. A solution to this system is necessary for generating angular scattering and energy-loss cross-section data. The cross-section data are then used to sample deflection cosine and energy-loss. The solution to the system in eq. (9) is similar to a Gauss quadrature system for an arbitrary weight function. Therefore, the method used to obtain a discrete cross-section for this work is an application of several Gauss quadrature algorithms. One procedure for obtaining a solution to system in eq. (9) is outlined below

1. Use the Modified Chebyshev Algorithm (MCA) [3] to map coefficients of classical orthogonal polynomials to coefficients of polynomials for an arbitrary weight function.
2. If using Radau quadrature (fixes one endpoint at 1), update Jacobi matrix according to Golub's description [5].
3. Apply Golub and Welsch algorithm [4] to obtain points and weights that are given by the eigenvalues and eigenvectors of the Jacobi matrix.

The MCA is used to map the recurrence coefficients (α,β) of a known classical orthogonal polynomial, $\pi(x)$, given by

$$\pi_{j+1}(x)=(x-\alpha_j)\pi_j(x)-\beta_j\pi_{j-1}(x) \tag{10}$$

to the recurrence coefficients (a,b) of an arbitrary set of polynomials, $p_l(x)$, that are given by

$$p_{l+1}(x)=(x-a_l)p_l(x)-b_l p_{l-1}(x). \tag{11}$$

The polynomials, $p_l(x)$, are orthogonal with respect to some arbitrary weight function, $w(x)$, and the modified moments of this weight function are

$$\chi_j=\int_a^b \pi_j(x)w(x) \tag{12}$$

The modified moments and the coefficients of the classical orthogonal polynomials are used as input to the MCA. The algorithm uses mixed moments,

$$\sigma_{k,l}=<p_k\,|\,\pi_l>=\int_a^b p_k(x)\pi_l(x)w(x)dx, \tag{13}$$

to relate the coefficients of the classical orthogonal polynomials to the desired orthogonal polynomials. Once the coefficients (a,b) are known the Jacobi matrix,

$$J=\begin{pmatrix} a_j & \sqrt{b_j} & 0 & \cdots & \cdots & 0 \\ \sqrt{b_j} & a_{j+1} & \sqrt{b_{j+1}} & & & \vdots \\ 0 & \sqrt{b_{j+1}} & a_{j+2} & \sqrt{b_{j+2}} & & \vdots \\ \vdots & & \ddots & \ddots & \ddots & 0 \\ \vdots & & & \sqrt{b_{N-2}} & a_{N-1} & \sqrt{b_{N-1}} \\ 0 & \cdots & \cdots & 0 & \sqrt{b_{N-1}} & a_N \end{pmatrix} \tag{14}$$

is formed. The eigenvalues of the Jacobi matrix correspond to the discrete points and the first entry of the eigenvectors squared corresponds to the discrete weights. If a Radau set is to be used the matrix given in eq. (14) must be modified according to Golub's description [4]. The following table gives an example of a discrete cross section for 1 MeV electrons in Carbon.

Table 1: Four Point Discrete Angular Deflection Cross Section Data

Discrete Deflection Cosine Point (ξ_n)	Discrete Deflection Cosine Weight (α_n)
-8.244431439774413e-01	2.010871029870031
1.885478581349338e-01	8.343040064585361
5.609457938047900e-01	5.179351598778211e+01
9.829897610014093e-01	7.507247294868574e+03

The cross section given in table 1 should preserve up to 2N-1 moments of the analog cross section since Radau quadrature can integrate polynomials up to order 2N-1. The following table gives moments of the analog cross section, moments calculated using the discrete cross section, and the relative difference between the two for the cross section in table 1.

Table 2: Moments of Four Point Discrete Angular-Deflection Cross-Section.

Order of Moment	Analog Moment	Discrete Moment	Relative Difference
0	9.293256144065792	9.293256144065797	501.0744e-018
1	9.291615893044463	9.291615893044472	877.0350e-018
2	9.288794923713871	9.288794923713887	1.7546e-015
3	9.284946297381490	9.284946297381518	3.0091e-015
4	9.280171953381741	9.280171953381785	4.7669e-015
5	9.274548248431435	9.274548248431500	7.1547e-015
6	9.268136174132964	9.268136174133055	9.9230e-015
7	9.260986466855453	9.261386787328156	43.2265e-006

Notice that the relative difference in the moments is exact to machine precision until the order 7 moment is reached. At this point, the higher-order moments are approximated in terms of the lower order moments.

The purpose of this method is to extend the mean free path of the particle while preserving moments of the cross-section. The cross-section given in table 1 began as an order five cross-section with one discrete point at $\mu = 1$. This point corresponds to a non-interaction. Specifically, it is the result of a collision with a nucleus that does not change the direction of the particle. Moreover, the probability of this interaction is several orders of magnitude more probable than for $\mu < 0.95$. The purpose of obtaining a cross-section with a point at $\mu = 1$ is because this point can be removed as it cancels with a term on the left-hand-side of the TE. Once the point and weight is removed the remaining weights are renormalized. The renormalized total cross-section is substantially smaller than the analog total cross section. Hence, the mean free path of a GBFP particle is extended. The process of removing the peaked portion of the cross section in a consistent manner is a regularization process.

The ratio of the mean free path of the discrete cross-section to the mean free path of the analog cross-section is used as a rough estimate of the speed-up gained by the GBFP method. The following figure gives this ratio for electrons of various energies in carbon. The ratio of the mean free path associated with angular deflection is given.

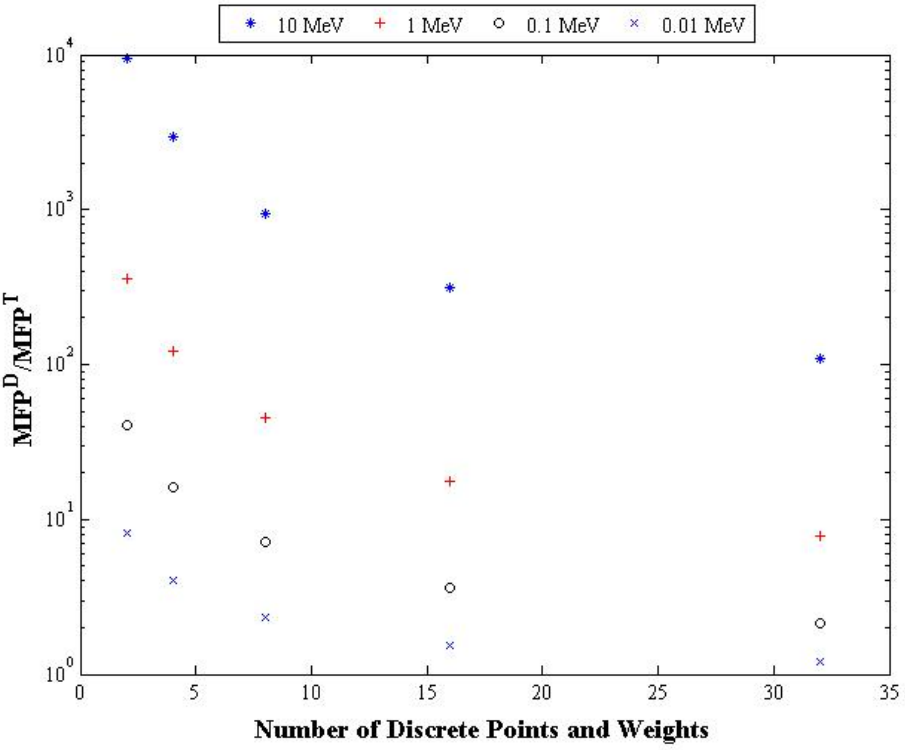

Figure 1. Ratio of Mean Free Path of GBFP Cross-Section to the Analog Cross-Section.

As seen in fig. 1, the largest gains in efficiency are at higher energies where the cross-section is substantially more peaked. As the number of points and weights increases, the ratio decreases

because as more points are added, the weight of the point near $\mu = 1$ decreases to correctly preserve moments. Figure 1 also indicates that there is a clear trade-off between accuracy and speed-up. However, previous studies [7] demonstrated that discrete cross-sections with just one angular deflection and energy-loss point and weight are accurate for integral quantities like dose.

3.2. IMPLEMENTATION OF THE GBFP DISCRETE MODEL IN GEANT4

Geant4 is a toolkit for the simulation of the passage of particles through matter. Its areas of application include high energy nuclear and accelerator physics, medical physics, and space physics [1]. A general use of Geant4 entails developing an application with at least three mandatory user-defined classes that are inherited from the base classes *G4VDetectorConstruction, G4VPhysicsList,* and, *G4VPrimaryGeneratorAction.* Creation of a *G4VDetectorConstruction* inheriting classes is used to set the problem geometry. In this inheriting class, the dimensions and material properties for the model are set. A *G4VPhysicsList* inheriting class is used to set the various physics processes that are applicable for the particles required by the simulation. In this inheriting class, the processes and the associated models are created and applied to the appropriate particles. Finally, creation of a *G4VPrimaryGeneratorAction* inheriting class is used to define the particle source. The position, energy, particle type, and direction are set in this class (distributions for each of these parameters can be used as well). It is at the level of processes and models where the GBFP method is implemented. A process and model must be written for each model (Discrete, Continuous, Hybrid) and for each interaction (angular deflection and energy-loss).

The implementation of the GBFP method occurs at the level of physics processes and models. For a typical user, these classes are not modified. The user selects from a list of processes and models and sets which physics will be used in the physics list. However, creation of processes and models for the GBFP method will require additional development. Analog and discrete GBFP processes and models are completed to date. The associated classes inherit from *G4VEmProcess* and *G4VEmModel.* The process class controls the ordering of interactions. For example, a process can be applied at the beginning of a step, along a step, and post-step. The process classes require an associated model. The models handle calculation of the total cross section for sampling distance to collision and methods for sampling quantities like angular deflection and energy-loss. The benefit of using Geant4 is gained through the modularity in the code package. As discussed, the implementation of the GBFP method only requires a description what interactions can occur and how to simulate these interactions. Beyond that, the code handles all of the other details and contains additional functionality like classes for extracting results and a sophisticated geometry modeling capability. The following figure shows a three-dimensional CEASE model captured with the Geant4 visualization tools. With the ability to easily adapt GBFP models and model sophisticated geometries for testing of the GBFP method, Geant4 is a clear choice.

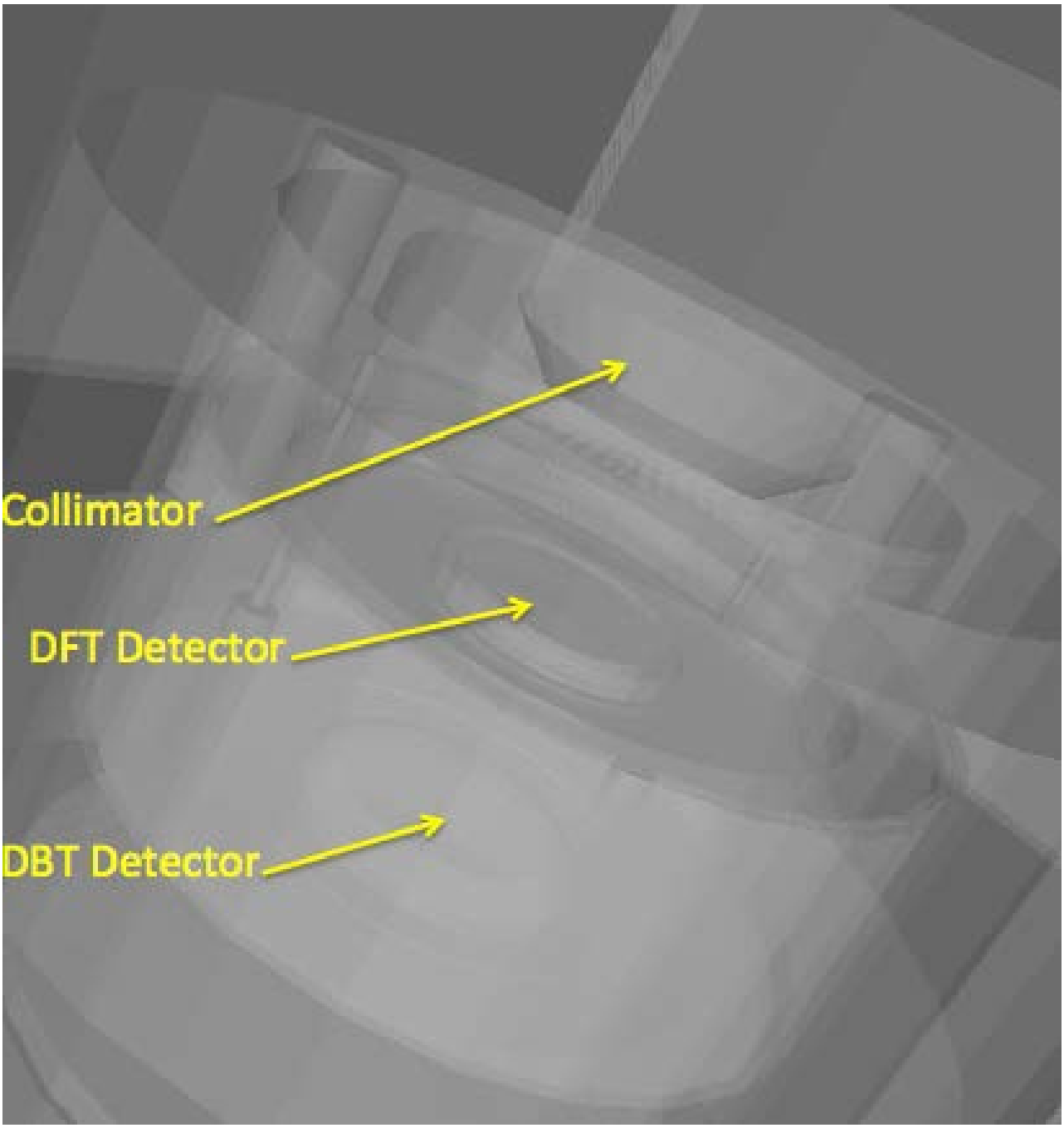

Figure 2. 3-D Rendering of Geant4 CEASE Detector Model.

4. RESULTS AND DISCUSSION

The following section presents results from initial testing of the GBFP discrete Model. The first several figures are angular distributions obtained using the GBFP discrete model and the analog model. Angular distributions were calculated for 1 MeV and 100 keV electrons in gold slabs. As seen in fig. 3, the discrete model cannot resolve angular distributions with two discrete angles in thin slabs.

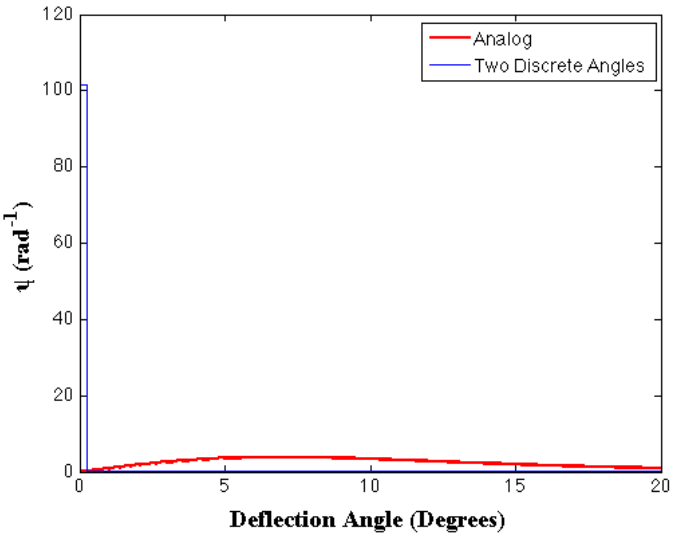

Figure 3. Comparison of Angular Distribution for 1 MeV Electrons in Gold.

However, increasing the number of angles increases the accuracy of the model and with enough points the discrete model can resolve angular distributions. Figure 4 presents a comparison of angular distributions for 1 MeV electrons in gold generated using a 32-point discrete model and the analog model. The discrete solution is in good agreement with the analog solution.

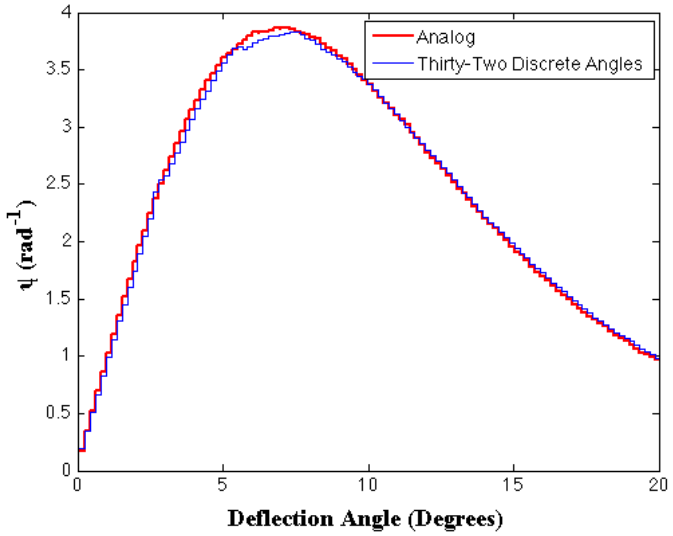

Figure 4. Comparison of Angular Distribution for 1 MeV Electrons in Gold.

Adding more points will improve the accuracy of the model. This indicates that the algorithm for generating the cross-section data and the implementation of the model was done correctly. Although these results are satisfactory, there are a couple limitations to the discrete model. First, for sufficiently low-energy particles, adding more points becomes impractical because efficiency gains are lost and the cross section set becomes cumbersome. Second, even a large number of points and weights does not help to resolve the angular distribution. Figure 5 presents a comparison of angular distributions for 100 keV electrons in gold generated using a 32-point discrete model to the analog model. Discrete artifacts are clearly seen in the figure. For this case, adding more points to resolve the angular distribution will result in a MFP that is on the order of the analog MFP.

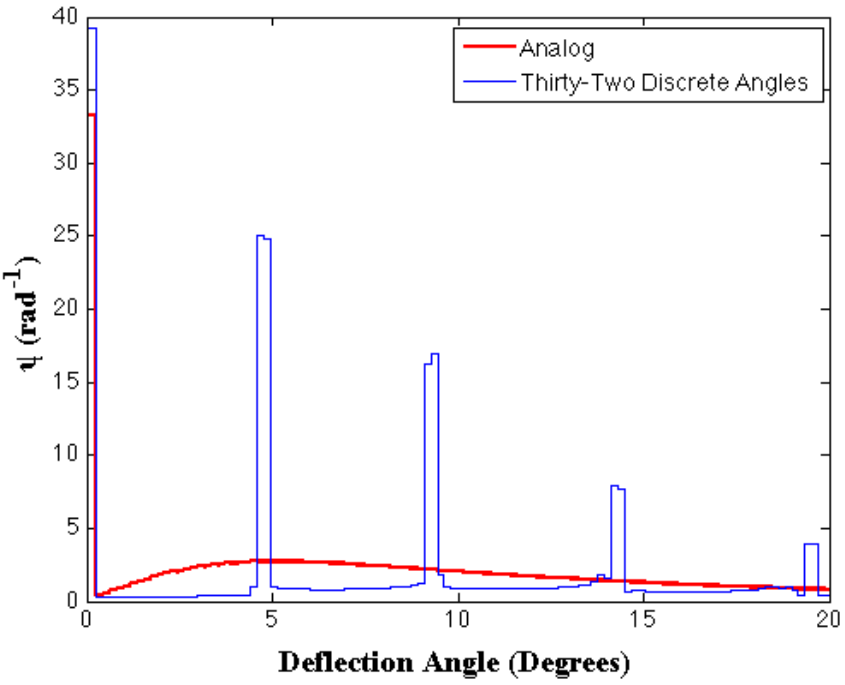

Figure 5. Comparison of Angular Distribution for 1 MeV Electrons in Gold.

Regardless of incident article energy and atom number, the GBFP discrete model generates inaccurate angular distributions when using lower order cross-sections or for sufficiently low-energy particles in thin slabs. Therefore, if quantities like angular distribution or energy spectrum are required, a hybrid method must be used to maintain efficiency while mitigating the discrete artifacts. The discrete artifacts arise because particles can only scatter into specific directions. The angular distributions tend to show a preference for these particular angles. Use of a continuous or hybrid model will resolve the discrete artifacts. Since the continuous and hybrid models are smooth or have a smooth component, the discrete artifacts are mitigated [10]. This is the motivation for using the hybrid or continuous models. However, discrete artifacts are not an issue for calculation of integral quantities like dose, so the discrete model is a good candidate for dose calculations.

The table below summarizes the computer time required to complete various dose calculations. As indicated in fig. 1 and in table 3, the greatest gains are achieved for higher energy source particles. However, the predicted speed-ups from fig. 1, which are estimated using MFP, are roughly a factor of 10 higher than the actual speed-ups based on computer time.

Table 3: GBFP Efficiency Gains Over Analog Monte Carlo.

Material	Energy (MeV)	Slab Width (mm)	Analog Calculation Computer Time (min)	GBFP Speed-up (Analog/GBFP)
Gold	1	0.1	147.1167	19.1061
Gold	0.1	0.1	16.3000	3.4077
Aluminum	1	5	591.0833	51.3986
Aluminum	0.1	0.5	76.5500	14.8161
Au/Al	0.25	0.004/0.096	54.1667	9.3660

It is important to note that each dose calculation was completed using only two discrete angles and one discrete energy loss, yet there is still good agreement between the analog and discrete solutions, as shown in Figures 6 through 13. Further accuracy can be gained by inclusion of more points and weights. Future reports will include details on the impact of the inclusion of more points and weights on the accuracy and efficiency of dose calculations.

In addition, dose profiles were calculated for a target with a high/low Z interface to demonstrate the accuracy of the method at interfaces, shown in Figures 14 and 15. The GBFP method is a single-event Monte Carlo method so boundary crossings algorithms are not necessary. A single-event method implies that it is a true Markov process. Therefore, what occurs at a collision site does not depend on how the particle arrived at the site. Moreover, a Markov process can be interrupted at any point and restarted without introducing error or correlation. For this reason, boundary crossings require stopping the particle at the boundary and then resampling distance to collision in the new material. This is not true of the condensed history algorithm because this approach is not a Markov process. As a result, condensed history algorithms require specific algorithms for handling boundary crossings and in some cases condensed history codes will switch over to analog Monte Carlo. Once the particle is far enough from the boundary, condensed history is resumed. None of these additional features are required for the GBFP method or single-event Monte Carlo.

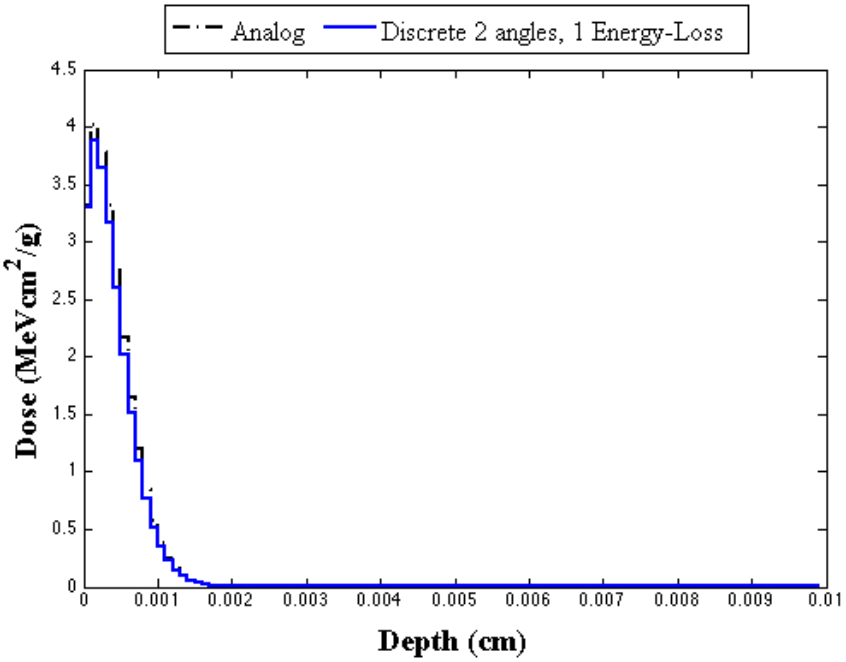

Figure 6. Comparison of Dose Profiles of 100 keV Electrons in Gold.

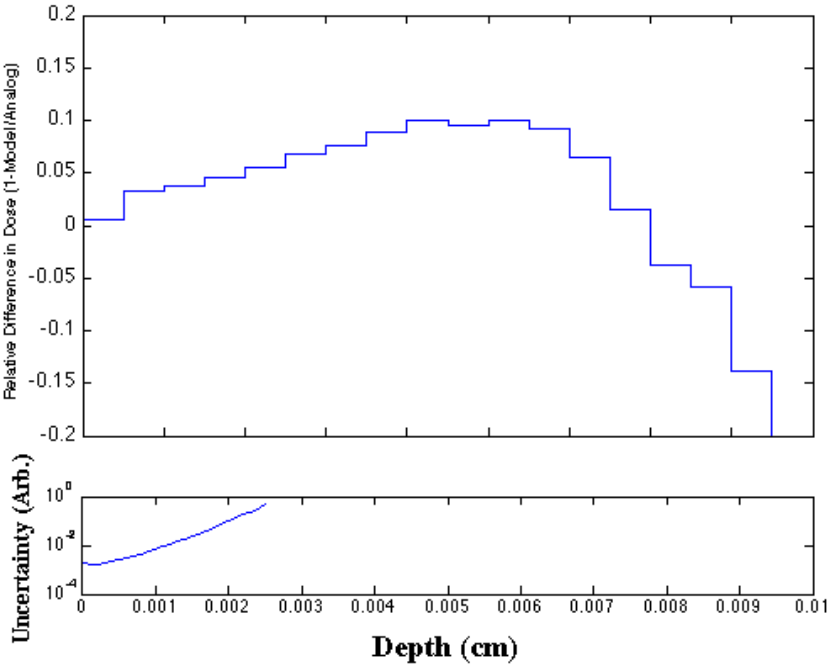

Figure 7. Relative Difference and Uncertainty in Dose Profile.

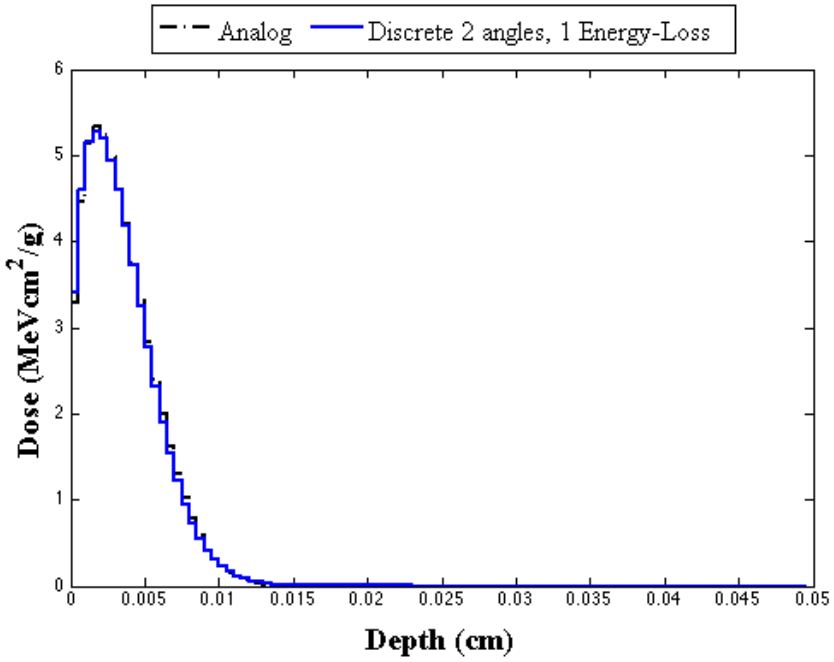

Figure 8. Comparison of Dose Profiles of 100 keV Electrons in Aluminum.

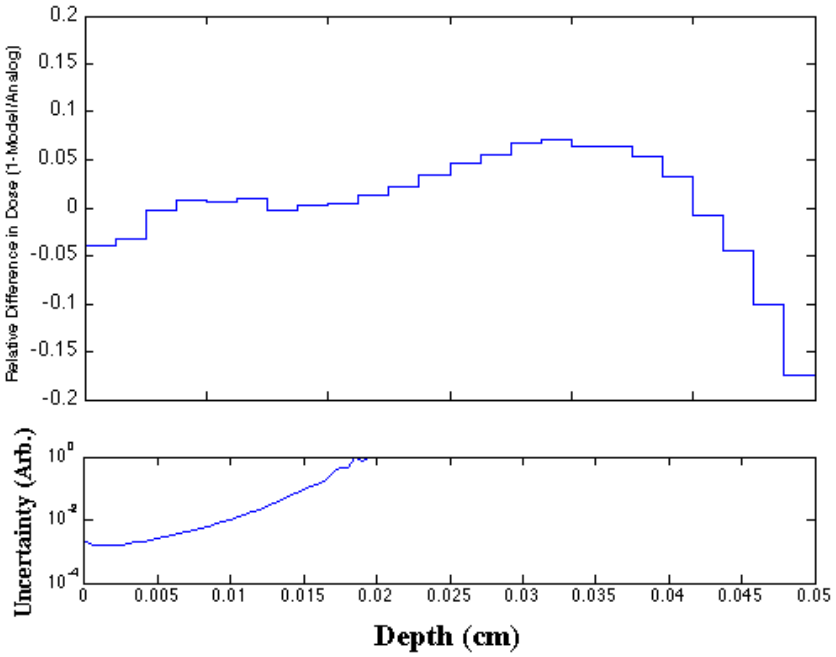

Figure 9. Relative Difference and Uncertainty in Dose Profile.

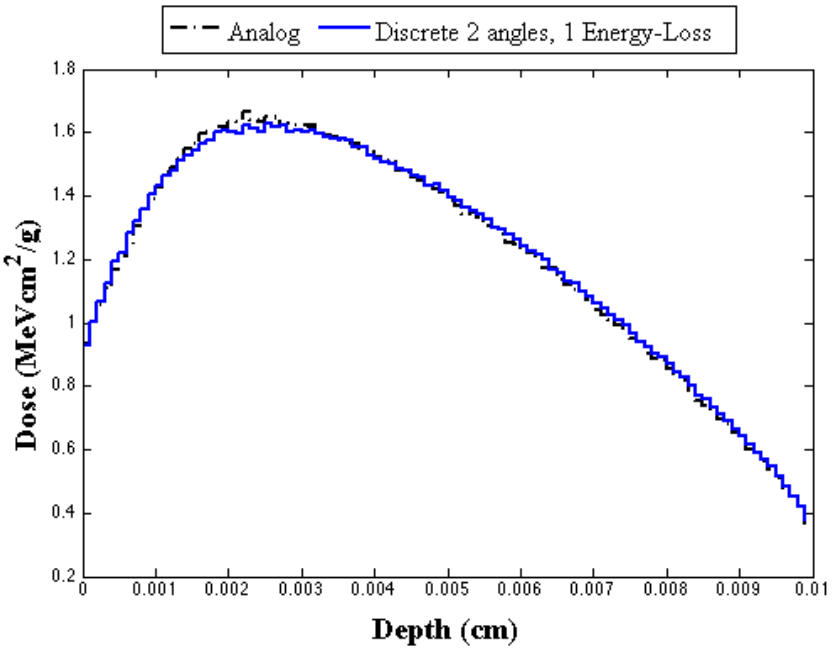

Figure 10. Comparison of Dose Profiles of 1 MeV Electrons in Gold.

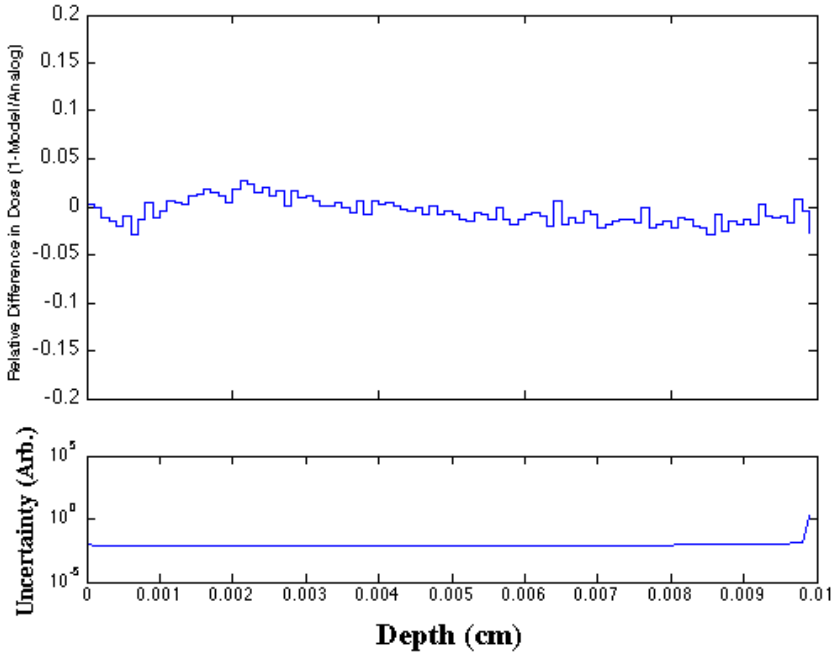

Figure 11. Relative Difference and Uncertainty in Dose Profile.

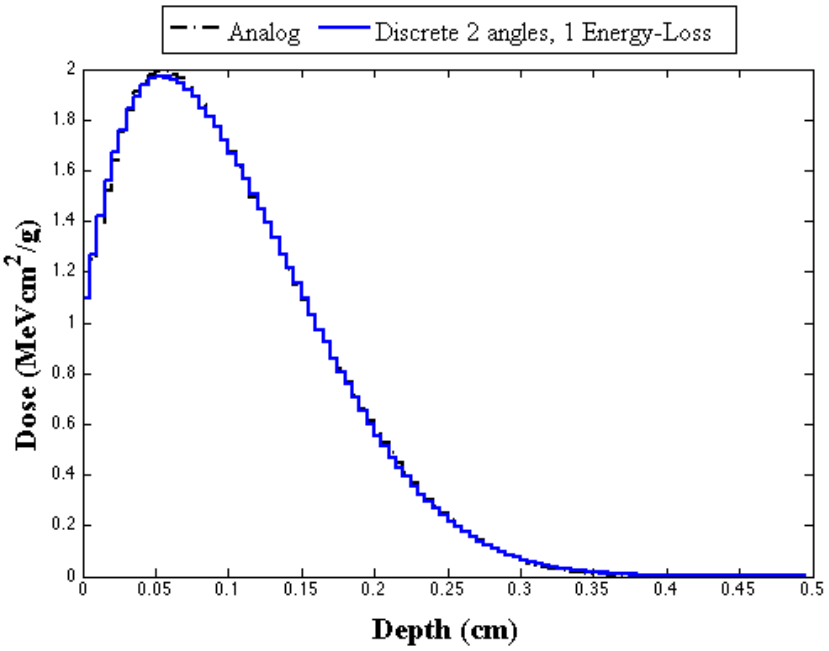

Figure 12. Comparison of Dose Profiles of 1 MeV Electrons in Aluminum.

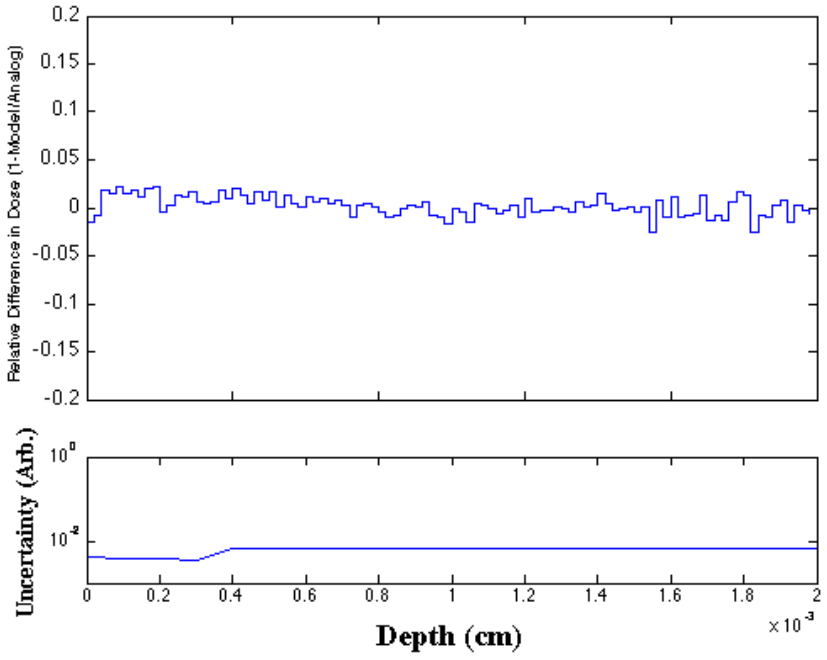

Figure 13. Relative Difference and Uncertainty in Dose.

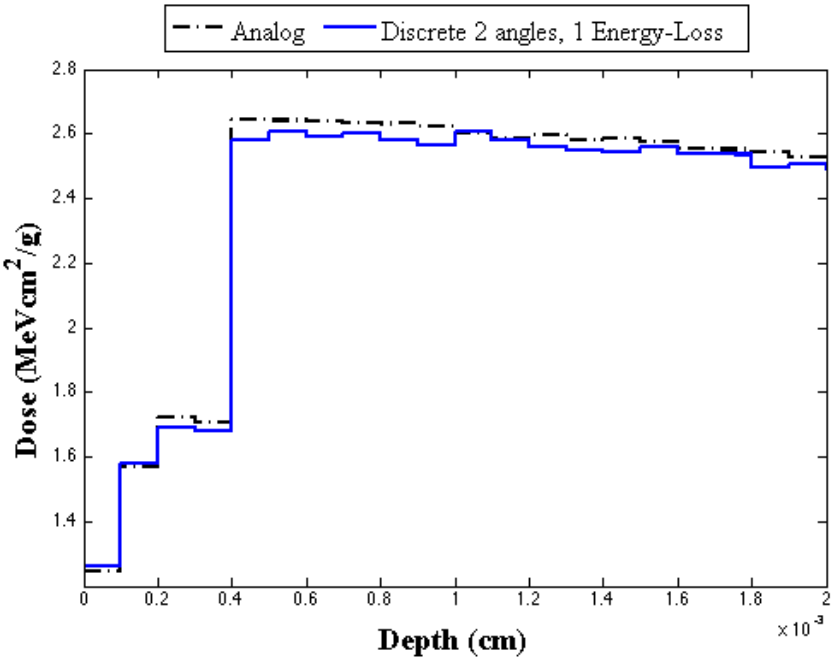

Figure 14. Dose Profiles of 250 keV Electrons in Slab with Gold-Aluminum Interface.

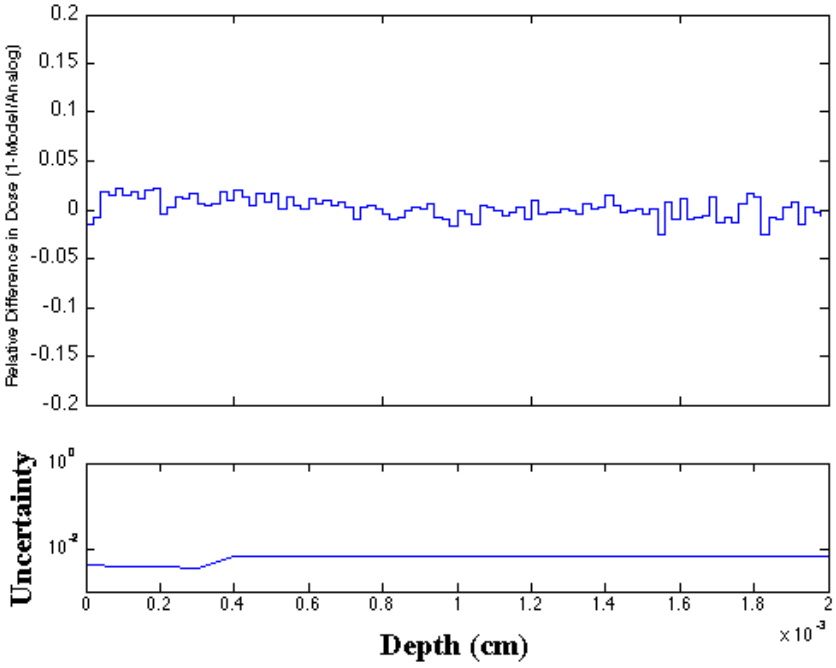

Figure 15. Relative Difference and Uncertainty in Dose Profile.

5. CONCLUSIONS

Significant progress was made towards implementation of the GBFP method in Geant4. Both the angular distribution results and the dose calculations indicate that the implementation was done correctly and that Geant4 is suitable for continuing GBFP research. In the case of angular distributions, it was demonstrated that the approximate solution approaches the analog solution by addition of more points and weights when approximating the cross-section. This behavior was expected and indicates that the algorithm for generating the cross-section data and the implementation of the model in Geant4 was successful. The agreement between the analog dose calculations and the discrete dose calculations provide further evidence a successful implementation of the discrete model.

Geant4 contains the necessary infrastructure for modeling a wide variety of problems. The ability to model sophisticated geometries will enable us to extend this work to multi-dimension problems that have not been explored. In addition, the existing multiple scattering and ionization processes and models will be used to compare the overall performance of the GBFP method to methods within Geant4 that are similar to condensed history.

Currently, analog and discrete GBFP models are implemented in Geant4. Implementation of the continuous and hybrid models will begin over the next reporting period. In addition, secondary electron production is not accounted for under the current GBFP model. Additional work must be completed to introduce secondary production and correlation of energy-loss and angular deflection for inelastic collisions with atomic electrons. Once each model is implemented and tested a consistent process for comparing geant4 standard multiple scattering and ionization models will be established. In addition, simulation of sophisticated geometries, like the CEASE detector, will begin once the models are implemented and tested.

REFERENCES

[1] Geant4, 2012, CERN, Accessed May 6th, 2013, http://geant4.cern.ch.

[2] Lewis, H. W., Multiple Scattering in an Infinite Medium, Physical Review, Volume 78, Number 5, June 1, 1950.

[3] Gautschi, W., Questions of Numerical Condition Related to Polynomials, Studies in Numerical Analysis, MAA Studies in Math, Volume 24, 1984.

[4] Golub, G. H., Calculation of Gauss Quadrature Rules, Mathematics of Computation, Volume 23, Number 106, April, 1969.

[5] Golub, G. H., Some Modified Matrix Eigenvalue Problems, Society for Industrial and Applied Mathematics, Volume 15, Number 2, April, 1973.

[6] Prinja, A. K., Moment-Preserving Computational Approach for High Energy Charged Particles, in Statement of Work, Broad Agency Announcement, Grant Award FA9453-11-1-0276, Air Force Research Laboratory, Kirtland AFB, NM, 2011.

[7] Franke, B. C. and A. K. Prinja, Monte Carlo Dose Calculations Using Discrete Scattering Angles and Discrete Energy Losses, Nucl. Sci. Eng., Volume 149, pp. 1-22, 2005.

[8] Leakeas, C. L. and E. W. Larsen, Generalized Fokker-Plank Approximations of Particle Transport with Highly Forward-Peaked Scattering, Nucl. Sci. Eng., Volume 137, pp. 236-250, 2001.

[9] Prinja, A. K. and B. C. Franke, A Regularized Boltzmann Collision Operator for Highly Forward Peaked Scattering, Trans. Am. Nucl. Soc., Volume 90, p. 281, 2004.

List of Acronyms

AFRL	Air Force Research Laboratory
CEASE	Compact Environmental Anomaly Sensor
GBFP	Generalized Boltzmann Fokker-Plank
MFP	Mean Free Path
UNM	University of New Mexico

DISTRIBUTION LIST

DTIC/OCP
8725 John J. Kingman Rd, Suite 0944
Ft Belvoir, VA 22060-6218 1 cy

AFRL/RVIL
Kirtland AFB, NM 87117-5776 2 cys

Official Record Copy
AFRL/RVBXR/Adrian Wheelock 1 cy

This page is intentionally left blank.